ЖЭТФ/JETP, 2026, том 169, вып. 5, стр. 567–575

MAGNETIC PROPERTIES OF THE RUDDLESDEN – POPPER PHASES $Pr_{2x}Sr_{3-2x}Ti_{2-x}Cu_xO_7$ ($x = 0.1, 0.2$)

D. V. Popov [a], ***I. V. Yatsyk*** [a], ***R. F. Likerov*** [a], ***R. B. Zaripov*** [a], ***R. M. Eremina*** [a,b*], ***R. G. Batulin*** [b], ***M. A. Cherosov*** [b], ***T. I. Chupakhina*** [c], ***Yu. A. Deeva*** [c], ***V. V. Bazhal*** [c], ***A. T. Gubaidullin*** [d]

[a] *Zavoisky Physical-Technical Institute FRC Kazan Scientific Center of the Russian Academy of Sciences 420029, Kazan, Russia*

[b] *Kazan Federal University 420008, Kazan, Russia*

[c] *Institute of Solid State Chemistry of the Ural Branch of the Russian Academy of Sciences 620990, Ekaterinburg, Russia*

[d] *Arbuzov Institute of Organic and Physical Chemistry FRC Kazan Scientific Center of the Russian Academy of Sciences 420088, Kazan, Russia*

Received December 09, 2025,
revised version December 10, 2025
Accepted for publication December 10, 2025

The Ruddlesden – Popper phases $Pr_{2x}Sr_{3-2x}Ti_{2-x}Cu_xO_7$ ($x = 0.1,\ 0.2$) were synthesized via a precursor method. The temperature dependence of the magnetic susceptibility in the studied non-stoichiometric compounds follows the Curie – Weiss law over the measured temperature range of 5–300 K, with no magnetic phase transitions. The temperature dependence of the electron paramagnetic resonance spectra was studied in the X- and Q-bands. The g-tensor components and linewidth were determined by fitting the electron paramagnetic resonance spectra of powder samples. The distance between the two vibronic levels of the paramagnetic centers was determined from the temperature dependence of the linewidth above 190 K.

Keywords: Ruddlesden – Popper phase, Jahn – Teller effect, vibronic levels

DOI: 10.31857/S0044451026050066

1. INTRODUCTION

The Jahn – Teller (JT) effect is a set of phenomena caused by the interaction of electrons with vibrations of atomic nuclei in molecules or solids in the presence of degeneracy of electronic states [1].The JT effect is characteristic of compounds containing ions of transition metals with a nonzero orbital momentum. In octahedral complexes, the effect is most pronounced when an odd number of electrons occupy the e_g orbitals. The pseudo-JT effect or the second-order JT effect is observed in compounds where spontaneous symmetry breaking in molecules and solids occurs, even when the corresponding electronic states are not degenerate. The static JT effect manifests itself when a Cu^{2+} ion with d^9 electron shell is placed in an octahedral environment of ligands. As a result of the JT effect, the octahedron becomes strongly elongated along the vertical axis: the two copper-ligand bonds become longer, while the four in-plane ones become shorter. The static distortion is fixed and observed in the crystal structure. As is known, a consequence of the electron-vibrational interaction in the octahedral Cu^{2+} complex is the spontaneous distortion of the octahedron along one of its fourth-order axes. In the adiabatic approximation, the tetragonally elongated configurations of the complexes correspond to the minima of potential energy. If the

* E-mail: REremina@yandex.ru

CuO_6 complex possesses small tetragonal or rhombic distortions, the minima of the adiabatic potential become energetically inequivalent. A situation is possible where these two parameters do not coincide. In the case of the dynamics JT effect, if the barriers between the minima are low and the temperature is high enough, the JT paramagnetic center in the crystal lattice begins to jump from one well to another, which manifests itself as a change in the direction of the octahedron axes. In the electron paramagnetic resonance (EPR) spectroscopy, this dynamics leads to a specific broadening of signals, as the local environment changes faster than the spin can feel the static field.

The JT effect is most pronounced in the EPR spectra of copper ions [2]. The comparison of bond lengths and the change in the effective g-factor with increasing temperature was performed in the work [3] and later in [4]. The temperature dependence of the probability of transition between different types of JT paramagnetic centers is determined by the Boltzmann distribution. Therefore, the two higher g-values vary with temperature because they represent weighted averages based on the relative population of the two vibrational levels, while the exchange rate between the levels is higher than the difference in their Zeeman energy. A model of this kind was used by Silver and Goetz [3] to explain the temperature dependence of the EPR spectrum of Cu^{2+} inserted in $K_2[Zn(H_2O)_6](SO_4)_2$. Measurements of the EPR spectra in the Q-band have shown that only two components of g-factor change with temperature. A line in the powder spectrum whose g-factor is minimal does not change its position with increasing temperature, and the g-factor values vary from 2.12 to 2.22 and from 2.42 to 2.32 as the temperature increases from 4 to 300 K.

The characteristic features in the temperature dependence of EPR spectra are determined by the energy distance between the potential minima related to temperature. For example, hyperfine structure lines are observed in the EPR spectrum of an impurity copper ion in the $ZnGa_2O_4$ compound [5]. With increasing temperature, these hyperfine EPR lines broaden significantly. At 560 K, the spectrum consists of an isotropic line with the following parameters: the g-factor $g = 2.116$ and the halfwidth at half maximum $\Delta H = 373$ Oe. This phenomenon is explained by transitions between the three levels of the adiabatic potential in octahedron.

As presented in [6], the JT effect in polar centers leads to a change in the character of the tetragonal-orthorhombic transition in $La_{2-x}M_xCuO_4$ systems as the concentration x increases. It has been shown that the cooperative JT effect is expressed in planar structures of the CuO_4 type.

In our opinion, the most promising compounds with JT effect are the Ruddlesden – Popper phases. The structure of the Ruddlesden – Popper phases of the $A_{n+1}B_nO_{3n+1}$ homologous series consists of n layers of perovskite ABO_3 separated by an AO layer with a rock salt structure, where A is alkali, alkaline-earth, or rare-earth metal, B is a transition metal. The Ruddlesden – Popper oxides host a remarkable set of properties including superconductivity, hybrid improper ferroelectricity, and negative thermal expansion [7]. It is also necessary to note their interesting dielectric properties, for example it was reported that this $La_{15/8}Sr_{1/8}NiO_4$ sample retains colossal dielectric constant more than 10000 well into the technically required gigahertz (GHz) frequency range [8].

Complex layered perovskite-like oxides $Sr_{n+1}Ti_nO_{3n+1}$ ($n = 1, 2$) are promising microwave dielectric materials. They are characterized by a moderate permittivity ($\varepsilon \approx 41-55$) and a low dielectric loss tangent. These strontium titanates are wide-bandgap semiconductors with a bandgap of ≈ 3.2 eV and are used as photocatalysts for hydrogen production via water splitting [9–11], as well as for the oxidation of toxic organic compounds to CO_2 and H_2O [12]. However, their photocatalytic activity is limited to the UV region.

Density functional theory calculations confirmed charge accumulation within the JT Cu^{2+} paramagnetic center doped in TiO_2 lattice [13], indicating more efficient separation and migration of photogenerated electron–hole pairs. For an Cu^{2+} impurity ion with orbital degeneracy, its energy states are shaped by the combined influence of the crystal field and the vibronic JT effect. The photocatalytic properties of compounds with the structure of the second homologue of the Ruddlesden – Popper series (presented in Fig. 1), namely $Sr_3Ti_2O_{7-\delta}$ can be enhanced by replacing strontium with praseodymium and simultaneously doping with a JT active ion such as copper.

A violation of the symmetry of the immediate environment should be expected for non-stoichiometric samples in which the positions of the ligand ions of the immediate environment of the $3d$ ion are not completely filled. The features of the JT effect in such compounds can be studied using the EPR method.

The aim of the present work is to study JT center in the newly synthesized non-stoichiometric perovskite-like oxides $Pr_{2x}S_{3-2x}Ti_{2-x}Cu_xO_7$ ($x = 0.1$, 0.2), which belong to the Ruddlesden – Popper series ($n = 2$), using X- and Q-band EPR spectroscopy and magnetometry.

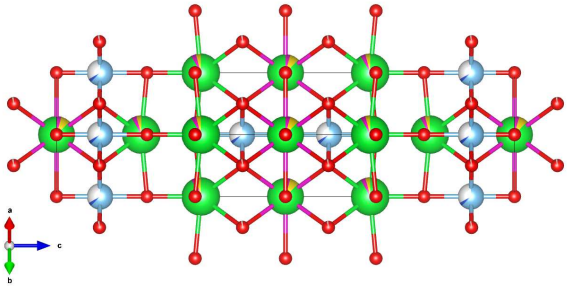

Fig. 1. Crystal structure of the $Pr_{2x}Sr_{3-2x}Ti_{2-x}Cu_xO_{7-\delta}$ ($x = 0.1, 0.2$) compound. Red orbs are oxygen ion, blue-silver orbs are Ti–Cu ionic positions, green-magenta-yellow orbs are Pr–Sr ionic positions. The figure was created using VESTA free software [14]

2. SAMPLE PREPARATION

$Pr_{0.2}Sr_{2.8}Ti_{1.9}Cu_{0.1}O_7$ and $Pr_{0.4}Sr_{2.6}Ti_{1.8}Cu_{0.2}O_7$ samples were synthesized by pyrolysis of nitrate-organic compositions of titanium isopropoxide $C_{12}H_{28}O_4Ti$, praseodymium oxide Pr_6O_{11}, strontium nitrate $Sr(NO_3)_2$, and copper oxide CuO [15]. The powder of $C_{12}H_{28}O_4Ti$ was weighed in a closed weighing bottle, then poured into a glass, and hydrolyzed with ethanol. The formed precipitate was titrated with nitric acid until dissolution, yielding titanyl nitrate $TiO(NO_3)_2$. Pr_6O_{11} and CuO comminuted weight of the substance calculated based on the amount of titanium isopropoxide were dissolved in dilute nitric acid (1:1) under gentle heating. $Sr(NO_3)_2$ was dissolved in distilled water. The resulting solutions were mixed, and a twofold excess of diammonium citrate $C_6H_{14}N_2O_7$ was added to the solution. The reaction mixture was evaporated at 400 °C until combustion began, accompanied by a tenfold increase in volume and the formation of a fine powder. The powder was transferred to a ceramic crucible and annealed at 950 °C to remove organic components. Next, stepwise annealing was carried out with a temperature increase of 50–100 °C until phase formation was complete. The composition of the obtained samples was monitored by X-ray phase analysis on a Shimadzu XRD-7000 S automatic diffractometer with a hold time of 5 s per point. X-ray diffraction patterns were processed using the FULLPROF-2021 program. Phase analysis of the reaction product was performed using the crystallographic database «Powder Standards Database - PDF2» (ICDD, USA, Release 2009). The obtained samples have the structure of the second homologue of the Ruddlesden – Popper series and do not contain any impurities of foreign phases.

3. EXPERIMENT

X-ray fluorescence (XRF) analysis were carried out on an Ekros XRF-9710 Pearl spectrometer with a Rh anode at 2 W (20 kV, 10 μA) in a helium gas flow. The exposure time was 30 s.

X-ray diffraction (XRD) was studied on Bruker D8 Advance automatic X-ray diffractometer equipped with a Vario attachment and a Vantec linear coordinate detector. Cu$K_{\alpha 1}$ radiation ($\lambda = 1.54063$ Å) was used, monochromated with a curved Johansson monochromator, the X-ray tube operating mode was 40 kV, 40 mA.

EPR spectra in X-band (working frequency $\nu = 9.4$ GHz) were measured on a Bruker EMX/Plus EPR spectrometer using an ER4122SHQE resonator and an Oxford purge cryostat for the temperature range of 5 to 150 K and a Bruker purge cryostat for the temperature range of 120 to 340 K. EPR spectra in Q-band ($\nu = 33.6$ GHz) were measured on a Elexsys E580 (Bruker) EPR spectrometer using an ER5106QTW resonator and an Oxford purge cryostat CF935 for the temperature range of 4.2 to 340 K. The temperature was maintained by the controller ITC503S (Oxford).

Magnetization measurements were performed on a Quantum Design PPMS-9 setup equipped with a vibrating magnetometer in two modes: field cooling (FC) and zero field cooling (ZFC).

4. RESULTS

XRF measurements established the actual composition of the samples as $Pr_{0.21}Sr_{2.79}Ti_{0.615}Cu_{0.055}O_{7-\delta}$ (Sample 1) and $Pr_{0.299}Sr_{2.701}Ti_{0.587}Cu_{0.103}O_{7-\delta}$ (Sample 2). The analysis shows the presence of some nonstoichiometry by oxygen as well as an impurity of europium ion of the order of one percent in both samples.

The refined XRD patterns, shown in Fig. 2, revealed that both compounds crystallize in the tetragonal space group I4/mmm with lattice parameters $a = b = 3.89406(11)$ Å, $c = 20.39810(11)$ Å($\chi^2 = 9.7647$) for Sample 1 and $a = b = 3.89999(7)$ Å, $c = 20.33100(7)$ Å($\chi^2 = 1.1954$) for Sample 2, respectively.

Ionic positions are listed in Table 1, and bond lengths are presented in Table 2. As can be seen from the Table 1, positions 1 and 2, which are occupied by strontium and praseodymium ions, are completely filled, however, there is a significant shortage of titanium ions in position 3 for Sample 1. For Sample 2, nonstoichiometry of filling positions is observed

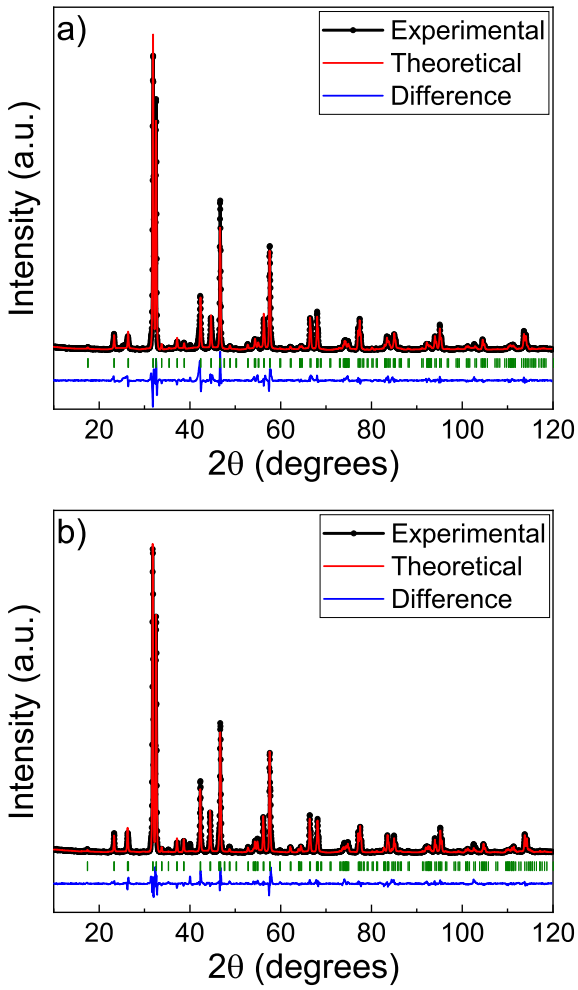

Fig. 2. Diffraction patterns for $Pr_{0.21}Sr_{2.79}Ti_{0.615}Cu_{0.055}O_{7-\delta}$ (*a*) and $Pr_{0.299}Sr_{2.701}Ti_{0.587}Cu_{0.103}O_{7-\delta}$ (*b*)

Table 1. Ionic position and occupation for two $Pr_{2x}Sr_{3-2x}Ti_{2-x}Cu_xO_{7-\delta}$ ($x = 0.1$, 0.2) samples

$Pr_{0.21}Sr_{2.79}Ti_{0.615}Cu_{0.055}O_{7-\delta}$					
Position	x	y	z	Ion	Occup.
1	0.000	0.000	0.500	Pr	0.177
				Sr	0.657
2	0.000	0.000	0.315	Pr	0.177
				Sr	0.657
3	0.000	0.000	0.095	Ti	0.489
				Cu	0.086
4	0.000	0.000	0.000	$O_{(1)}$	1.0
5	0.000	0.000	0.199	$O_{(2)}$	0.95
6	0.000	0.500	0.095	$O_{(3)}$	0.948
$Pr_{0.299}Sr_{2.701}Ti_{0.587}Cu_{0.103}O_{7-\delta}$					
Position	x	y	z	Ion	Occup.
1	0.000	0.000	0.500	Pr	0.187
				Sr	0.527
2	0.000	0.000	0.315	Pr	0.187
				Sr	0.527
3	0.000	0.000	0.095	Ti	0.419
				Cu	0.074
4	0.000	0.000	0.000	$O_{(1)}$	1.0
5	0.000	0.000	0.187	$O_{(2)}$	0.857
6	0.000	0.500	0.096	$O_{(3)}$	0.857

Table 2. Bond length between metal ions and oxygen in the $Pr_{2x}Sr_{3-2x}Ti_{2-x}Cu_xO_{7-\delta}$ samples

Sample	Position	$O_{(1)}$	$O_{(2)}$	$O_{(3)}$
1	1	2.753(1) Å	–	2.74(1) Å
	2	–	2.77(2) Å	2.68(2) Å
	3	1.94(3) Å	2.11(2) Å	1.95(1) Å
2	1	2.75(1) Å	–	2.66(1) Å
	2	–	2.60(1) Å	2.66(1) Å
	3	1.93(1) Å	1.87(1) Å	1.95(1) Å

for both praseodymium and titanium ions. Such a strong nonstoichiometry of filling positions leads to a strong distortion of the immediate environment formed by oxygen ions in the octahedron.

4.1. Magnetization

Figure 3 shows the results of magnetization measurements on the $Pr_{2x}Sr_{3-2x}Ti_{2-x}Cu_xO_{7-\delta}$ ($x = 0.1$, 0.2) samples. No features were detected in the temperature dependences of the inverse magnetic susceptibility, indicating the absence of structural and phase transitions in the selected temperature range, in consistence with the results of EPR studies of the samples (Fig. 4).

The paramagnetic (linear) part of the obtained data was approximated according to the Curie – Weiss law

$$\chi = \frac{C}{T - \Theta_{CW}},$$

where C is the Curie constant and Θ_{CW} is the Curie – Weiss temperature [16]. The fitting parameters are presented in Table 3. A negative Curie – Weiss temperature indicates the predominance of antiferromagnetic interactions between copper spins in the samples. Us-

Table 3. The Curie – Weiss temperature, the Curie constant and the effective magnetic moment in the $Pr_{2x}Sr_{3-2x}Ti_{2-x}Cu_xO_{7-\delta}$ samples

Sample	Θ_{CW}, K	C, $\frac{K \cdot emu}{mol}$	μ_{eff}, μ_B	μ_{eff}^{th}, μ_B
1	-38	0.26	1.44	1.10
2	-38	0.48	1.96	1.19

ing the obtained Curie constants, the effective magnetic moment was calculated by formula

$$\mu_{eff} = \sqrt{\frac{3k_B C}{N_A}},$$

where k_B is a Boltzmann constant, N_A is an Avogadro number. The obtained values of the effective magnetic moment are given in Table 3.

The theoretical effective magnetic moment μ_{eff}^{th} was calculated from the composition of the samples, determined from XRF analysis using formula

$$\left(\mu_{eff}^{th}\right)^2 = \sum_i N_i g_i^2 S_i (S_i + 1)$$

where N_i, g_i, and S_i are the concentration, the g-factor, and the spin of every individual magnetic ion of the compound including an admixture of europium ions. The resulting values are presented in Table 3 as well. It should be noted, that the theoretical effective magnetic moment is lower than the experimental one for both compounds. This discrepancy may be due to the presence of defects and magnetic impurities in the samples, as well as a change in the valence of titanium ions from 4+ to 3+ which is unlikely due to oxygen deficiency in the samples. The lines in the EPR spectrum from titanium 3+ are superimposed on the lines from copper ions, so it is not possible to distinguish their contribution when registering spectra in the microwave X- and Q-bands.

4.2. Electron paramagnetic resonance

The EPR spectra in the Q-band for both samples are shown in Fig. 4. The data were obtained in a wide temperature range from 5 to 340 K. For a single paramagnetic center of a copper ion, one expects to observe lines from the hyperfine interaction with the nuclear spin of copper ($I = 3/2$) in the EPR spectrum. However, these hyperfine lines are not detected in EPR spectra for Sample 1 and Sample 2, which indicates the presence of an exchange interaction between the spins of copper ions in the studied samples. It can be

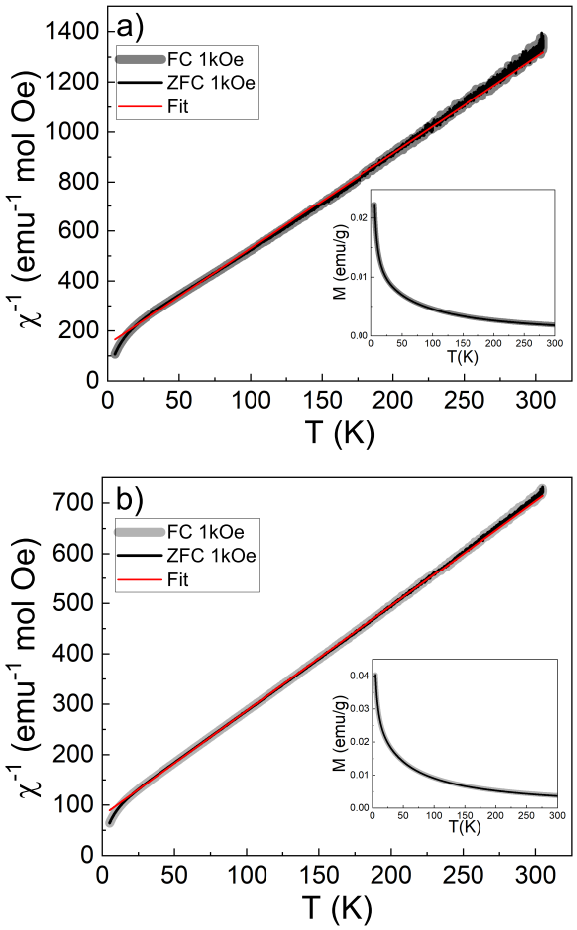

Fig. 3. Temperature dependences of the inverse magnetic susceptibility for $Pr_{0.21}Sr_{2.79}Ti_{0.615}Cu_{0.055}O_{7-\delta}$ (*a*) and $Pr_{0.299}Sr_{2.701}Ti_{0.587}Cu_{0.103}O_{7-\delta}$ (*b*). Insets show temperature dependences of the magnetization. Red lines are the Curie – Weiss approximation of the paramagnetic part

assumed that copper ions form clusters for which the cooperative JT effect may be observed.

At low temperatures, the EPR spectrum acquires a shape, characteristic of a powder sample. Due to averaging over crystallite orientations, a single line in the form of the first derivative of the absorption existing in the crystal, is replaced by a complex absorption spectrum visualized as a combination of the derivatives of three different spectral modes. It is particularly evident for the resonance spectrum observed in the Q-band while the X-band powder spectrum is poorly resolved. Therefore, the analysis presented below is based solely on data obtained in the Q-band. The EPR line shape for a powder sample is approximated by summing the microwave absorption contributions from crystallites that are randomly oriented in all direction. The line shape was calculated for the geometry in which the

external magnetic field was perpendicular to the microwave magnetic field. The line shape was defined as the first derivative of the following analytical expression with respect to the magnetic field [17]:

$$F = \sum_{i>j} W_{ij} f_{ij}$$

(the summation is taken over different transitions between i and j ion levels and can be omitted for Cu^{2+} ion). Here

$$W \propto \left[\frac{g_x^2 g_y^2}{g_\perp^2} + \frac{g_z^2}{g^2} \left(\frac{\left(g_\perp^2 - g_x^2\right)\left(g_y^2 - g_\perp^2\right)}{g_\perp^2} \cos^2\Theta + g_\perp^2 \right) \right]$$

is the probability of an allowed transition between neighboring levels,

$$g_\perp^2 = g_x^2 \sin^2\phi + g_y^2 \cos^2\phi,$$
$$g^2 = g_\perp^2 \sin^2\Theta + g_z^2 \cos^2\Theta,$$

where g_x, g_y, g_z are the g-tensor components of the paramagnetic center Cu^{2+}. The function f determines the shape of the absorption line for a paramagnetic center and is given by the expression

$$f = \frac{\Delta H + \alpha(H - H_{\rm res})}{(H - H_{\rm res})^2 + \Delta H^2} + \frac{\Delta H - \alpha(H + H_{\rm res})}{(H + H_{\rm res})^2 + \Delta H^2}.$$

Here $H_{\rm res} = h\nu/g\mu_{\rm B}$ (h is a Planck constant) is the resonance line position, ΔH is the linewidth [18, 19] with three components ΔH_x, ΔH_y, ΔH_z for three principal directions of the external field, and α is an asymmetry parameter (determined with the accuracy ± 0.01). Angles Θ and ϕ determine the direction of the magnetic field with respect to crystallographic axes of the crystallites. The averaging of the linewidth ΔH over crystallite orientations is analogous to that for g-factors. The need to use a non-zero value of the parameter α may be related to the conductive properties of the sample or the presence of exchange interactions [20].

The temperature dependences of the linewidth and the effective g-factor for Q-band data are shown for both samples in Fig. 5 and 6, respectively.

As can be seen from the Figs. 5 and 6, the values of the g-factors of the Sample 1 and Sample 2 are close but do not coincide, which indicates a different degree of distortion of the octahedra formed by surrounding oxygen ions. The components of the g-tensor at 100 K are equal $g_z = 2.28 \pm 0.01$, $g_y = 2.18 \pm 0.005$, $g_x = 2.07 \pm 0.002$ for the Sample 1 and $g_z = 2.29 \pm 0.01$, $g_y = 2.14 \pm 0.005$, $g_x = 2.05 \pm 0.002$ for the Sample 2, respectively. The accuracy of determining the linewidth

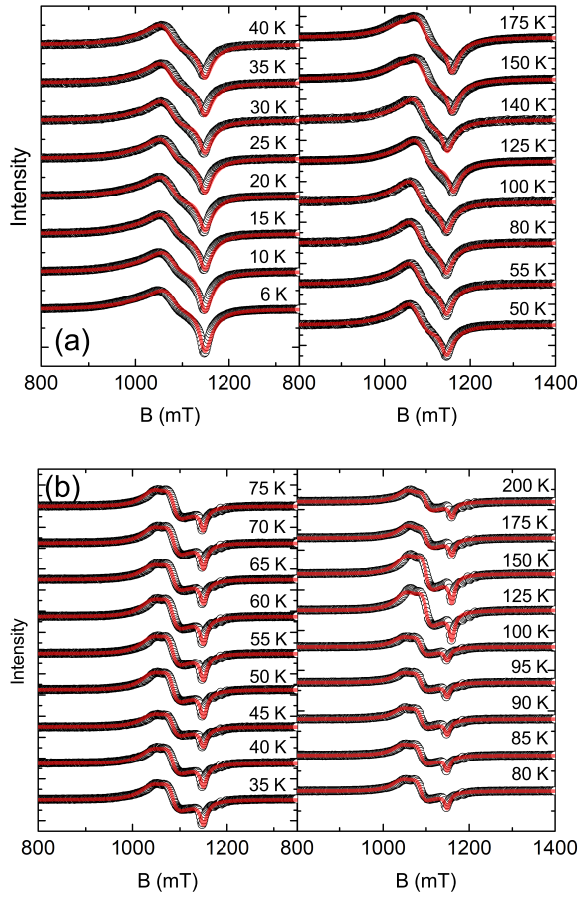

Fig. 4. EPR lines (symbols) for $Pr_{0.21}Sr_{2.79}Ti_{0.615}Cu_{0.055}O_{7-\delta}$ (*a*) and $Pr_{0.299}Sr_{2.701}Ti_{0.587}Cu_{0.103}O_{7-\delta}$ (*b*), and their approximations (lines)

was about 2.6%. These values are close to the ones obtained for Cu^{2+} ions in the octahedral environment [21] and with similar behavior as well [22]. As the temperature is increased from 6 to 30 K, the g_z value for ESR line in the Sample 1 is observed to decrease significantly from 2.36 to 2.29, while the linewidth ΔH_z is narrowed from 650 to 450 Oe. This behavior is attributed to the influence of antiferromagnetic fluctuations. Although no magnetic ordering was detected in the temperature dependence of the magnetic susceptibility, a deviation from linearity was recorded in the inverse susceptibility data with respect to the Curie–Weiss approximation. At a temperature of about 150 K, a change in trend is observed in the temperature dependence of the g-factor: its value increases from 2.29 to 2.32. Starting from the same temperature, a broadening of the EPR line is recorded on further heating.

The lowest g-value practically does not change with temperature, showing that the local structure of the paramagnetic center does not change from the tetrag-

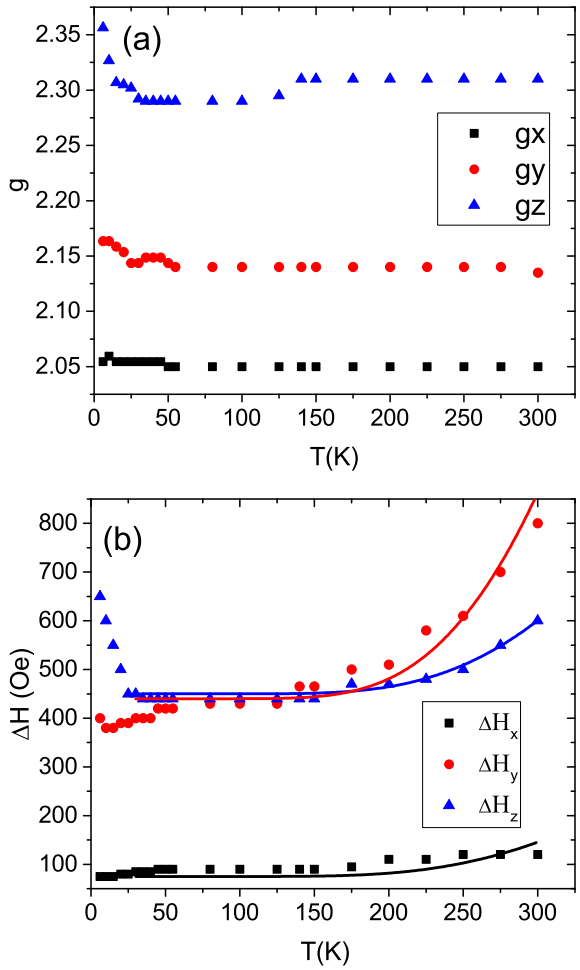

Fig. 5. g-factor (a) and linewidth (b) components of EPR line for $Pr_{0.21}Sr_{2.79}Ti_{0.615}Cu_{0.055}O_{7-\delta}$. Lines are the approximations of the linewidths by formula (1) with the parameters: for ΔH_x — $\Delta H_{x0} = 85 \pm 2$ Oe, $A_x = 8500 \pm 500$ Oe (black line), for ΔH_y — $\Delta H_{y0} = 440 \pm 5$ Oe, $A_y = 20000 \pm 1000$ Oe (red line), for ΔH_z — $\Delta H_{z0} = 430 \pm 10$ Oe, $A_z = 50000 \pm 2000$ Oe (blue line); $\Delta E = 1400 \pm 20$ K

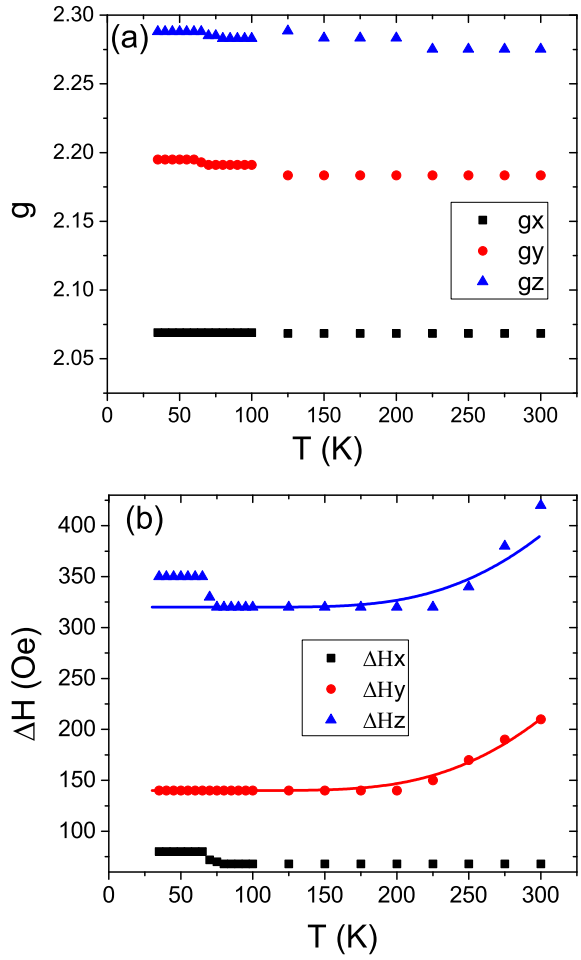

Fig. 6. g-factor (a) and linewidth (b) components of EPR line for $Pr_{0.299}Sr_{2.701}Ti_{0.587}Cu_{0.103}O_{7-\delta}$. Lines are the approximations of the linewidths by formula (1) with the parameters: for ΔH_y — $\Delta H_{y0} = 140 \pm 5$ Oe, (red line), for ΔH_z — $\Delta H_{z0} = 320 \pm 10$ Oe (blue line); $A = 7500 \pm 100$ Oe, $\Delta E = 1400 \pm 20$ K

onally elongated ground state $d_{x^2-y^2}$ towards a tetragonally compressed geometry $d_{3z^2-r^2}$. The small deviation in the data for g_x component at lower temperatures is in agreement with the findings in [3].

5. DISCUSSION

It should be noted that the linewidth broadens with temperature over the range from 150 to 300 K. We associate this behavior with the JT effect of the Cu^{2+} ions in an octahedral oxygen environment [23], since JT distortion is rather frequent in Ruddlesden – Popper phase compounds, specifically in Cu-containing samples [7]. A thermally activated change in the linewidth at high temperatures based solely on spin relaxation and requires consideration of an additional broadening mechanism. A similar activated process was observed, in particular, in the one-dimensional $CuSb_2O_6$ magnet, TiOCl, and the kagome antiferromagnet vesignite [24].

The behavior of the linewidths for Sample 1 and Sample 2 is slightly different. We attribute the difference in the ΔH_y and ΔH_z linewidth in the studied samples to the different concentrations of trivalent praseodymium and divalent strontium near which the paramagnetic copper centers are located. Disorder in the crystal field, resulting from the statistically random distribution of Pr and Sr ions in the distant coordination spheres of Cu ions, broadens the potential minima by an energy ΔE of the order of 100 cm^{-1}, which was

shown for the $LaSrAl_{1-x}Cu_xO_{4-\delta}$ sample in [25]. This leads to the lowering of one minimum which correspond to elongation of the CuO_6 octahedron along the z-axis or two minima (elongation along the x- and y-) of the adiabatic potential. Along each Cu–O bond direction, two stable positions for planar and apical oxygen ions emerge, shifted relative to the center by approximately 0.2 Å (see Table 2).

The adiabatic potential for an Cu^{2+} impurity center in a samples features several equivalent wells. Provided that the barriers between them are not excessively high, the Cu^{2+} ion can move from well to well via tunneling or over-barrier jumps. Whereas the probabilities of tunneling transitions from the ground vibrational state in one well to the ground state in an adjacent well are expected to be largely temperature-independent, the probabilities of over-barrier jumps ΔE grow exponentially with increasing temperature.

The observed sharp increase in linewidth with temperature can be attributed to a thermally activated dynamic JT process. In the range from 100 to 300 K, we describe the EPR linewidth using the formula [26]

$$\Delta H = \Delta H_0 + A \cdot \exp\left(-\frac{\Delta E}{T}\right). \qquad (1)$$

where the coefficient A is a prefactor. For simplicity, we neglected its temperature dependence, as it varies very slowly compared to the exponential factor. Figs. 5 6 show good agreement between the simulation results and the experimental EPR linewidth data. The activation energy ΔE obtained from the fitting procedure is near 1400 ± 20 K both for $Pr_{0.21}Sr_{2.79}Ti_{0.615}Cu_{0.055}O_{7-\delta}$ and for $Pr_{0.299}Sr_{2.701}Ti_{0.587}Cu_{0.103}O_{7-\delta}$. The obtained values of the residual linewidth along the x-, y-, and z-axes are given in the captions to Figs. 5 and 6 for Samples 1 and 2, respectively. The residual EPR linewidth ΔH_0 is due to anisotropic exchange interactions between copper spins. The magnitudes of the coefficient A are given in the captions to the Figs. 5 and 6, respectively. The linewidth remains almost unchanged for the x-component of the powder spectrum. The magnitude of coefficient A varies with the direction. This is probably due to the anisotropic properties of the Ruddlesden – Popper phase where $c/a = 5.218$. A similar anisotropy was observed in thermal conductivity in $Sr_2Nb_2O_7$ [27]. The authors suggested that this arises from the natural superlattice formed by alternating blocks, which constitute the layered structure.

The temperature dependence of the linewidth in the studied compounds is similar to the behavior in $CuSb_2O_6$, where the linewidth shows no signs of saturation up to 500 K. Since the dynamic JT regime is realized, the relaxation process via phonons is dominant. This situation was described for the two-dimensional case and is valid for $CuSb_2O_6$ due to the square planar lattice of copper in the trirutile structure, especially considering that only the asymptotic high-temperature behavior is taken into account [28].

The ground state splitting $2E_{\rm JT} = 1540$ K in $CuSb_2O_6$ [28] is in good agreement with our determined energy gap ΔE for $Pr_{0.21}Sr_{2.79}Ti_{0.615}Cu_{0.055}O_{7-\delta}$ and $Pr_{0.299}Sr_{2.701}Ti_{0.587}Cu_{0.103}O_{7-\delta}$ compounds. This value is in agreement with the result reported in [26] for Cu^{2+} doped in $LiNbO_3$, where the energy barrier value between the adiabatic potential minima was obtained from exponential broadening of the EPR signal at $T > 200$ K, which was $\Delta E = 0.15$ eV. It should be noted that the energy barrier values for the compounds $Pr_{0.21}Sr_{2.79}Ti_{0.615}Cu_{0.055}O_{7-\delta}$ and $Pr_{0.299}Sr_{2.701}Ti_{0.587}Cu_{0.103}O_{7-\delta}$ and those obtained in [26] and [28] are approximately the same and are determined by the structure of the JT paramagnetic centers formed by the copper ion in the oxygen octahedron.

6. CONCLUSION

The compounds $Pr_{2x}Sr_{3-2x}Ti_{2-x}Cu_xO_{7-\delta}$ ($x = 0.1, 0.2$) were synthesized by pyrolysis of nitrateorganic compositions. Their actual compositions, determined by XRF analysis, were found to be $Pr_{0.21}Sr_{2.79}Ti_{0.615}Cu_{0.055}O_{7-\delta}$ and $Pr_{0.299}Sr_{2.701}Ti_{0.587}Cu_{0.103}O_{7-\delta}$, respectively. Diffraction analysis showed that the compounds had a structure of $Sr_3Ti_2O_{7-\delta}$ type with a lack of filling of titanium positions for both samples and strontium positions for Sample 2. Magnetization measurements showed no specific transition temperatures in the range of 5–300 K. A Curie – Weiss fit revealed negative Curie – Weiss temperatures for both compounds, indicating the predominance of antiferromagnetic interactions between copper spins. EPR measurements revealed the presence of Jahn – Teller effects in both $Pr_{0.21}Sr_{2.79}Ti_{0.615}Cu_{0.055}O_{7-\delta}$ and $Pr_{0.299}Sr_{2.701}Ti_{0.587}Cu_{0.103}O_{7-\delta}$ samples. The energy barrier values between distorted configurations of the Jahn – Teller paramagnetic copper centers for the Sample 1 and Sample 2 are obtained from the temperature dependence of the EPR linewidth.

Acknowledgments. The authors are grateful to A. I. Smirnov for useful discussions. The work was supported by the Russian Science Foundation (grant

No. 24-23-20123) and the Government of the Sverdlovsk Region.

Conflict of interest. The authors of this work declare that they have no conflict of interest.

Authors' contribution. The contribution of the authors is equal.

REFERENCES

1. K. I. Kugel and D. I. Khomskii, Sov. Phys. Usp. **25**, 231 (1982).

2. W. Bietsch, A. Mirea, T. Kamleiter, M. Weiss, U. S. Schubert, C. H. Weidl, C. Eschbaumer, I. Ovchinnikov, and N. Domracheva, Mol. Phys. **100**, 1957 (2002).

3. B. L. Silver and D. Getz, J. Chem. Phys **61**, 638 (1974).

4. M. A. Hitchman, W. Maaskant, J. van der Plas, C.J. Simmons, and H. Stratemeier, J. Amer. Chem. Soc. **121**, 1488 (1999).

5. A. M. Vorotynov, G. A. Petrakovskii, K. A. Sablina, A. F. Bovina, and A. D. Vasilev, Phys. Solid State **52**, 2415 (2010).

6. A. S. Moskvin and Y. D. Panov, Phys. Status Solidi B **212**, 41 (1999).

7. A. Herlihy, W.-T. Chen, C. Ritter, Y.-C. Chuang, and M. S. Senn, J. Amer. Chem. Soc. **147**, 7209 (2025).

8. S. Krohns, P. Lunkenheimer, C. Kant, A. V. Pronin, H. B. Brom, A. A. Nugroho, M. Diantoro, and A. Loidl, Appl. Phys. Lett. **94**, 122903 (2009).

9. H. Zhang, S. Ni, Y. L. Mi, and X. X. Xu, J. Catal. **359**, 112 (2018).

10. X. Sun, Y. Xie, F. Wu, H. Chen, M. Lv, S. Ni, G. Liu, and X. Xu, Inorg. Chem. **54**, 7445 (2015).

11. X. Sun and X. Xu, Appl. Catal. B Environ. **210**, 149 (2017).

12. A. Sorkh-Kaman-Zadeh and A. Dashtbozorg, J. Mol. Liq. **223**, 921 (2016).

13. P. P. Tang, X. Y. Zhang, J. Zai, J. S. Chen, W. Zhang, and X. Wei, J. Phys. Chem. C **127**, 5552 (2023).

14. K. Momma and F. Izumi, J. Appl. Crystallogr. **44**, 1272 (2011).

15. T. I. Chupakhina, Y. A. Deeva, N. V. Melnikova, V. V. Gorin, I. S. Sivkov, and O. I. Gyrdasova, Mendeleev Commun. **29**, 349 (2019).

16. D. V. Popov, R. G. Batulin, M. A. Cherosov, I. V. Yatsyk, I. V. Yanilkin, E. M. Moshkina, A. T. Gubaidullin, D. I. Fazlizhanova, and R. M. Eremina, J. Alloys Compd. **1040**, 183213 (2025).

17. G. M. Zhidomirov, Y. S. Lebedev, S. N. Dobryakov, N. Y. Shteinshneider, A. K. Chirkov, and V. A. Gubanov, *Interpretation of Complex EPR Spectra*, Nauka, Moscow (1975).

18. D. V. Popov, R. G. Batulin, M. A. Cherosov, I. V. Yatsyk, T. I. Chupakhina, Yu. A. Deeva, A. S. Makarchenko, D. I. Fazlizhanova, V. A. Shustov, R. M. Eremina, and T. Maiti, J. Alloys Compd. **1009**, 176900 (2024).

19. D. V. Popov, R. G. Batulin, M. A. Cherosov, I. V. Yatsyk, T. I. Chupakhina, Y. A. Deeva, R. M. Eremina, and T. Maiti, Magn. Reson. Solids **25**, 23301-9 (2024).

20. J. P. Joshi and S. V. Bhat, J. Magn. Res. **168**, 284 (2004).

21. A. M. Vorotynov, G. A. Petrakovskii, K. A. Sablina, A. F. Bovina, and A. D. Vasilev, Phys. Solid State **52**, 2415 (2010).

22. A. Prokhorov, K. Lamonova, R. Minikayev, J. Lančok, and A. Prokhorov, Eur. Phys. J. Plus **137**, 1349 (2022).

23. D. Reinen and C. Friebel, in *Structural Problems*, Springer, Berlin, Heidelberg (2005), p. 1.

24. S. H. Do, J. van To, H. D. Zhou, and K. Y. Choi, Phys. Rev. B **90**, 104426 (2014).

25. Y. V. Yablokov, T. A. Ivanova, and A. E. Usachev, Phys. Solid State **40**, 569 (1998).

26. A. K. Petrosyan, R. M. Khachatryan, and E. G. Sharoyan, Phys. Status Solidi B **122**, 725 (1984).

27. T. D. Sparks, P. A. Fuierer, and D. R. Clarke, J. Amer. Cer. Soc. **93**, 1136 (2010).

28. M. Heinrich, H. A. Krug von Nidda, A. Krimmel, A. Loidl, R. M. Eremina, A. D. Ineev, B. I. Kochelaev, A. V. Prokofiev, and W. Assmus, Phys. Rev. B **67**, 224418 (2003).